HHS Public Access

Author manuscript

Biomaterials. Author manuscript; available in PMC 2023 January 04.

Published in final edited form as:

Biomaterials. 2020 October ; 255: 120149. doi:10.1016/j.biomaterials.2020.120149.

Biomimetic and Estrogenic Fibers Promote Tissue Repair in Mice and Human Skin via Estrogen Receptor β

Seungkuk Ahn,

Christophe O. Chantre,

Herdeline Ann M. Ardoña,

Grant M. Gonzalez,

Patrick H. Campbell,

Kevin Kit Parker*

Disease Biophysics Group, John A. Paulson School of Engineering and Applied Sciences, Harvard University, Cambridge, MA 02138

Abstract

The dynamic changes in estrogen levels throughout aging and during the menstrual cycle influence wound healing. Elevated estrogen levels during the pre-ovulation phase accelerate tissue repair, whereas reduced estrogen levels in post-menopausal women lead to slow healing. Although previous reports have shown that estrogen may potentiate healing by triggering the estrogen receptor (ER)-β signaling pathway, its binding to ER-α has been associated with severe collateral effects and has therefore limited its use as a therapeutic agent. To this end, soy phytoestrogens, which preferentially bind to the ER-β, are currently being explored as a safer therapeutic alternative to estrogen. However, the development and evaluation of phytoestrogen-based materials

***Corresponding author:** Kevin Kit Parker, 29 Oxford St. (Rm. 321) Cambridge, MA, 02138, Tel: (617) 495-2850, Fax: (617) 495-9837, kkparker@seas.harvard.edu.

Author contributions

S.A. and K.K.P. designed the study. S.A. performed and analyzed data related to scaffold fabrication, characterization, and wound healing experiments. C. O. C. and G. M. G. designed the use of hyaluronic acid backbone via iRJS machine. C. O. C. and P. H. C. supported in vivo mouse wound healing experiments. H. A. M. A. supported *ex vivo* human skin wound healing experiments. S.A. and K.K.P. prepared illustrations and wrote the manuscript. C. O. C. and H. A. M. A. contributed to manuscript writing.

Credit Author Statement

Seungkuk Ahn: Conceptualization, Methodology, Investigation, Formal analysis, Data curation, Visualization, Writing- Original draft preparation, Writing - Review & Editing, Project administration. **Christophe O. Chantre:** Methodology, Investigation, Writing- Original draft preparation, Writing - Review & Editing. **Herdeline Ann M. Ardoña:** Methodology, Investigation, Writing- Original draft preparation, Writing - Review & Editing. **Grant M. Gonzalez:** Methodology, Investigation. **Patrick H. Campbell:** Methodology, Investigation. **Kevin Kit Parker:** Conceptualization, Supervision, Writing- Original draft preparation, Writing - Review & Editing, Project administration, Funding acquisition.

Appendix A. Supplementary data

Supplementary data related to this article can be found online.

Conflict of interests

The authors declare no competing financial interests.

Declaration of interests

The authors declare that they have no known competing financial interests or personal relationships that could have appeared to influence the work reported in this paper.

as local ER-β modulators remains largely unexplored. Here, we engineered biomimetic and estrogenic nanofiber wound dressings built from soy protein isolate (SPI) and hyaluronic acid (HA) using immersion rotary jet spinning. These engineered scaffolds were shown to successfully recapitulate the native dermal architecture, while delivering an ER-β-triggering phytoestrogen (genistein). When tested in ovariectomized mouse and *ex vivo* human skin tissues, HA/SPI scaffolds outperformed controls (no treatment or HA only scaffolds) towards promoting cutaneous tissue repair. These improved healing outcomes were prevented when the ER-β pathway was genetically or chemically inhibited. Our findings suggest that estrogenic fibrous scaffolds facilitate skin repair by ER-β activation.

Keywords

Soy Phytoestrogen; Immersion Rotary Jet Spinning; Nanofiber; Wound Healing; Estrogen Receptor β

1. Introduction

Estrogen, the primary female sex hormone, affects the regulation and development of various organs—including skin [1]. During the menstrual cycle, estrogen levels rise before ovulation and fall after ovulation [2]. Recent clinical studies have reported that women who undergo surgery during pre-ovulatory phase show a decreased incidence of wound rupture and hypertrophic scarring regardless of age, race, and ethnicity [3]. In contrast, post-menopausal estrogen deficiencies cause delayed or impaired wound healing in elderly women [4–6]. These hormonal events can be modulated when estrogen binds to estrogen receptors (ERs: ER-α or ER-β), activating downstream signaling pathways [7, 8].

In cutaneous microenvironments, ER-β is expressed throughout the skin (*e.g.*, epidermal keratinocytes, dermal fibroblasts, and cutaneous appendages) [9]. Previously, the role of ERs in wound healing has been determined using estrogen-deficient (*e.g.,* ovariectomized (OVX) mouse) and ER knockout (KO) rodent models, revealing that estrogen accelerates skin repair by stimulating the ER-β signaling pathway [8, 10]. Unfortunately, estrogen also activates the ER-α signaling pathway which may potentiate pathologies (*e.g.*, blood clots and higher risk of breast cancer progression) [11, 12]. A compound that can selectively activate the ER-β signaling pathway might thereby emerge as a promising alternative to estrogen for the development of more potent and safer regenerative therapies in wound care.

Interestingly, phytoestrogens found in soy are structurally and functionally analogous to estrogen [13]. Among soy phytoestrogens, genistein is a selective estrogen receptor modulator that preferentially binds to ER-β [14, 15]. Preclinical and clinical studies have both shown that topical treatments and oral intake of genistein accelerate skin tissue repair (*e.g.*, new granulation tissue and hair follicle formation) in animal models and human patients [16–18]. While previous studies established the protective roles of phytoestrogens in the wound healing process [16–18], engineering soy phytoestrogen scaffolds as local ER-β modulators and activators towards skin repair remain unexplored. To this end, we hypothesized that soy-based fibrous scaffolds may expedite cutaneous wound healing by triggering the ER-β pathway, while providing an extracellular matrix (ECM)-mimetic

microenvironment and allowing for local delivery of genistein into a target region. We herein engineered hyaluronic acid (HA) and soy protein isolate (SPI) composite fibers using immersion rotary jet spinning (iRJS) [19–21]. The spun HA/SPI fibers were able to recapitulate skin ECM microenvironment and deliver genistein. When applied to OVX wild-type (WT) mouse and *ex vivo* human skin models, HA/SPI scaffolds promoted stronger skin tissue repair than controls (no treatment or HA only scaffolds). These beneficial effects were abrogated when the ER-β signaling pathway was inhibited.

2. Materials and Methods

2.1. Fiber fabrication.

Soy protein isolate (PRO-FAM® 974, ADM) and hyaluronic acid sodium salt (MW: 1500–1800 kDa, Sigma) were dissolved in UltraPure DNase/RNase-free distilled water (Invitrogen) and DMSO (Sigma) (6:1) solution with 10 mg/mL of sodium chloride (Sigma) and stirred overnight. The nanofibers were spun from the polymer solution by using iRJS as previously reported [21]. The soy/polymer composite solution was injected at a speed of 10 mL/min into the reservoir and extruded through the orifices (with a diameter of 300 μm) into the precipitation bath (80% ethanol) at 15,000 RPM. The precipitated fibers were then collected on the rotating mandrel in the bath. The spun fibers were crosslinked with 10 mM EDC and 4 mM NHS in 80% ethanol for 24 hrs on a shaker. The crosslinked fibers were washed by running DI water for 1 h, frozen in DI water at −80 ºC, and freeze-dried using lyophilizer (SP Scientific) for further characterization and wound healing studies.

2.2. Scanning electron microscopy (SEM) and fiber morphology analysis.

The freeze-dried samples were sputter-coated with Pt/Pd (Denton Vacuum) prior to imaging. The samples were then imaged by field emission scanning electron microscopy (FESEM, Carl Zeiss). The SEM images of fiber samples were processed in ImageJ (NIH) software, together with DiameterJ plug-in to calculate for fiber diameter and porosity [22]. For energy-dispersive X-ray spectroscopy (EDS), carbon (C_K) and sulfur (S_K) atoms were mapped with the corresponding SE2 images in FESEM.

2.3. Rheology testing

TA Instruments Discovery Hybrid 3 Rheometer with a cone plate geometry was used to determine the rheological properties of solutions (HA (2% wt/v) and HA/SPI (2%/2% wt/v)). The cone had a 60 mm diameter, 2° angle, and 56 μm truncation gap. The plate was temperature-controlled to 25 °C. A solvent trap was used to minimize solvent evaporation during testing.

2.4. Uniaxial tensile testing

The freeze-dried samples were uniaxially pulled at a strain rate of 5 %/s up to 60 % strain in a tensile tester (CellScale Biotester – Biaxial Tester). The data were recorded using a built-in software (CellScale) and analyzed using OriginPro 8.6 software (OriginLab).

2.5. Fourier-transform infrared spectroscopy (FTIR)

FTIR spectra of samples were obtained by using attenuated total reflectance (ATR)-FTIR (Bruker). Scan range was set between 600 and 4000 cm^{-1}, with 16 scans at a resolution of 2 cm^{-1} per sample. The recorded data were normalized to C-O-C stretching peak of HA at around 1050 cm^{-1} using OriginPro 8.6 software.

2.6. Swelling measurement

The scaffolds were submerged and incubated in PBS solution at 37 °C. The weight of scaffolds in the solution was measured at day 0, 1, 2, 3, and 4 of swelling. The swelling ratio was then calculated by comparing the weight increase compared to the initial weight of the scaffolds.

2.7. In vitro degradation test.

Degradation of scaffolds were tested by submerging the scaffolds in phosphate-buffered saline (PBS, Invitrogen) solution in 6 well plates at 37 ºC and 5% CO_2 with or without hyaluronidase (1 U), following a previously established method [23–25]. The change in weights of the scaffolds at the given time was measured compared to the initial weight of the scaffolds at day 0. The complete degradation time was tracked for all test scaffolds.

2.8. Liquid chromatography-mass spectrometry (LC-MS).

LC-MS (Agilent) was utilized to quantify the amount of genistein within scaffolds. Samples were dissolved in DMSO, filtered with polytetrafluorethylene (PTFE) membranes (Pall Corporation), and loaded in the system. For the LC part, we used a C18 LC column (ZORBAX RRHD StableBond 80Å C18, 2.1 × 100 mm, 1.8 μm, 1200 bar pressure limit) with a gradient of H_2O and acetonitrile (ACN) at a flow rate of 0.25 mL/min. The gradient started with 95% H_2O and 5% ACN, and the ratio increased to 100% ACN. The chromatographically separated molecules then underwent electrospray ionization (ESI) in selected ion monitoring (SIM) mode to detect the charged ions according to their molecular weights ($[genistein+H]^+$ at *m/z* 271). For analyzing the genistein release profile, the crosslinked HA/SPI fibers were submerged in PBS solution at 37 ºC and 5% CO_2. At a given time, the remaining scaffolds and PBS solution were separately collected, dried, dissolved in DMSO, and then subjected LC-MS analysis to measure the amount of genistein.

2.9. In vitro cytotoxicity testing

The cytotoxicity of the scaffolds was evaluated by using a standard lactate dehydrogenase (LDH) cytotoxicity assay [26]. In brief, human neonatal dermal fibroblasts (HNDFs, Angio-Proteomie) were cultured on the scaffolds for 24 hours at 37 ºC and 5% CO_2 with Dulbecco's modified eagle medium (DMEM, Thermo Fisher Scientific) and antibiotics (penicillin-streptomycin, Thermo Fisher Scientific, diluted to 1%). Following the manufacturer's protocol, cell culture solutions were collected and then incubated with the reaction and stop reagents from the assay kit. Absorbance at 490 nm was recorded using a plate reader (Synergy HT; BioTek, NJ, USA).

2.10. ER-β binding assay

The ER-β binding affinity of genistein released from HA/SPI dope and scaffolds was measured using a commercial binding assay kit (LanthaScreen TR-FRET ER-β competitive binding assay kit, Thermo Fisher Scientific) by the manufacturer's service team (SelectSreen Services, Thermo Fisher Scientific). The HA/SPI dope was prepared by dissolving HA/SPI (2%/2% wt/v) in DMSO. On the other hand, HA/SPI scaffolds were submerged in DMSO for 5 days to allow for genistein to be released in the supernatant. The samples (HA/SPI dope and supernatant from scaffold incubation) were then diluted in 1% DMSO to the working concentrations, and mixed with assay buffer, target/antibody mixture, and tracer. The mixture was incubated for 60 mins at room temperature. In addition, 0% (without 17-β-estradiol) and 100% (the highest concentration of 17-β-estradiol) displacement control (DC) were prepared as negative and positive control samples. The fluorescence emissions at 495 (for terbium) and 520 (fluorescein) nm were recorded using a plate reader. Then, emission ratio was calculated by dividing fluorescein emission at 520 nm by terbium emission at 495 nm. Finally, the ER-β binding affinity (% displacement, DC) was calculated according to the following equation:

$$\text{Binding affinity}\left(\%\ \text{displacement}\right) = \frac{(\text{emission ratio of 0\% DC - emission ratio of sample})}{(\text{emission ratio of 0\% DC - emission ratio of 100\% DC})}$$

Z′-factor was also calculated to verify the robustness of the assay as previously described [27], where the Z'-factor higher than 0.5 demonstrates a robust assay. The Z'-factor for all data points were 0.74, which confirmed the validity of the binding affinity assay results.

2.11. Mouse excisional wound splinting model.

All animal experiments (protocol ID: 11–11-2) were approved by Harvard Institutional Animal Care and Use Committee (IACUC). As previously reported [28], we performed the mouse excisional splinting model to recapitulate human-mimetic healing processes in mouse by preventing wound contraction in mouse skin. WT female mice (7 weeks old, C57BL/6, Charles River Laboratories) and ER-β knock-out female mice (7 weeks old, B6.129P2-Esr2tm1Unc/J, Jackson Laboratory) were fed a soy-free special diet (LabDiet 5V5R 50/IF, PMI® Nutrition International) and ovariectomized by manufacturers. After the ovariectomy surgery, mice were delivered and acclimated to the vivarium for a week. In addition, we also performed wound healing experiments using WT female mice (7 weeks old, C57BL/6, Charles River Laboratories) without ovariectomy to verify whether additional released genistein and HA-based biomimetic scaffold could promote skin tissue healing in normal mice.

After a week of acclimation to the vivarium, wound clips were removed to allow the mice to recover for another week before the wound healing surgeries were conducted. On the day of wound healing surgery, isoflurane was used to anesthetize the mice throughout the procedure. Hair on the dorsal side of mice was shaved by using an electric razor, followed by cleaning their skin with betadine (Santa Cruz Biotechnology) and 70% ethanol (v/v). The full thickness wounds were inflicted on each mice by using a 6-mm diameter sterile biopsy punch (Integra Miltex). Before the surgery, splinting rings were prepared from a silicon

sheet (Grace Bio-Labs) by cutting 8 mm inner holes with an 8-mm sterile biopsy punch (Integra Miltex), sterilized with 70% ethanol (v/v) and under UV light in a sterile cell culture hood. We applied the splinting rings to the wound site with a synthetic adhesive (Krazy glue) and surgical suture (Ethicon). Nanofiber scaffolds were placed to the wounds and secured with Tegaderm (Nexcare) patches. Control wounds did not receive any treatment but were covered with Tegaderm. At day 20 post-injury, mice were sacrificed and skin tissues were harvested via IACUC approved protocols. Power analysis was applied to the mice model using G power software (Table S1) as previously reported [29, 30]. The calculated statistical power values were higher than 0.9 for all conditions, which support the validity of our *in vivo* experiments.

2.12. Human skin wound model.

Human skin biopsies with 2 mm wounds (NativeSkin®, Genoskin) were prepared according to manufacturer's protocol, as previously reported [31]. The human skin model used in this study was produced from skin samples collected at the Cape Cod Hospital (Hyannis, MA, USA), through the "Genoskin Tissue Donation Program". This human tissue sourcing program has been approved by the Cape Cod Healthcare Institutional Review Board (CCHC IRB).

The skin biopsies were obtained from the abdomen of two different patients (44 years old and 39 years old, female), wounded with a 2-mm diameter biopsy punch, and embedded within a proprietary nourishing hydrogel in 12-well Transwell inserts. Upon receipt from the manufacturer, human skin biopsies were incubated with their dedicated culture medium for 1 h at 37 ºC, 5% CO_2, and humidity.

Afterwards, nanofiber scaffolds were cut with 2-mm diameter biopsy punch and applied to the wound sites. The skin biopsies were cultured for 7 days (the maximum possible culture time recommended by the manufacturer) whereby the culture medium was changed daily. Tissues were then harvested 7 days post-injury. In an effort to specifically block ER-β pathway *in vitro*, an ER-β antagonist (4-[2-phenyl-5,7-bis(trifluoromethyl)pyrazolo[1,5-a]pyrimidin-3-yl]phenol, PHTPP, Sigma) was added to the culture medium. Following a previously reported concentration used for an *in vitro* experiment [32], 10 mM PHTPP stock solution was prepared in DMSO and diluted to a 0.01 mM working concentration in the culture medium. To eliminate the effect of the vehicle (DMSO) on the healing process, the same amount of vehicle solution was also added to the culture medium of control samples.

2.13. Histological analysis of skin tissues.

The harvested skin tissues were fixed with 4% (v/v) paraformaldehyde (PFA) in PBS solution overnight at 4 ºC and washed by PBS 3 times. Along with a series of graded alcohol washes (from 0 % to 100 %), the fixed tissues were processed for paraffin embedding, sectioning, and Masson's trichrome staining at the Harvard Specialized Histopathology Core. A slide scanner (Olympus VS120) was used to image the Masson's trichrome stained tissues. Dermal wound gap and neo-epidermis length for mouse skin, as well as re-epithelialization for human skin, were calculated based on the Masson's trichrome images processed in ImageJ software. Following previously established methods [33, 34],

the dermal wound gap and neo-epidermis length were analyzed by measuring the distance between the advancing edges of dermal or epidermal layers, respectively (μm). The re-epithelialization was calculated by measuring distance among the edges of newly formed epithelial layers. The sample numbers were as follows: 1) n=4 in the normal mouse model without ovariectomy, 2) n=10 for the control and HA/SPI group, n=8 for the HA group in the OVX WT mouse model, 3) n=6 for the control and HA/SPI group, n=5 for the HA group in the OVX ER-β KO mouse model, and 4) n=9 for the control group, n=8 for the HA group, n=9 for the HA/SPI group, and n=8 for the HA/SPI+PHTPP group with 2 sections per tissue from 2 different patients in the human skin model.

2.14. Immunofluorescent analysis of skin tissues.

The paraffin-processed sections were de-paraffinized by sequentially washing the sections with xylene (Sigma) and ethanol: water gradient. The de-praffinized sections were incubated with 5% bovine serum albumin (BSA, Jackson Immunoresearch) in PBS for 2 hrs at room temperature, followed by primary antibodies (anti-cytokeratin 14 (K14) and anti-ER-β, Abcam) in 1% BSA in PBS overnight at 4 ºC. After the primary antibody incubation, the samples were washed with PBS 3 times, followed by incubation with secondary antibodies (Alexa Fluor 488-conjugated anti-rabbit IgG (H+L) secondary antibody, Alexa Fluor 594-conjugated anti-mouse IgG (H+L) secondary antibody, and 4orexa Fluor 488-conjugated a (DAPI), Thermo Fisher Scientific)) in 1% BSA in PBS for 1 h at room temperature. Subsequently, the samples were washed with PBS 3 times and mounted with Prolong Gold anti-fade agent (Invitrogen) on glass coverslips. A spinning disc confocal microscope (Olympus ix83) was used to image the processed samples. For coverage analysis, the positively stained area in the wound sites and total wound area were measured using ImageJ software. The sample numbers for the analysis were n=8 for the control group, n=7 for the HA group, n=10 for the HA/SPI group in the OVX WT mouse model, as well as n=6 for the control and HA/SPI group, n=5 for the HA group in the OVX ER-β KO mouse model.

Skin Tissue Architecture Quality (STAQ) index, developed in Python (v 2.5, Python), was used for quantitative immunofluorescence staining analysis, as previously reported [35, 36].

2.15. Statistical analysis.

Box plots were used to present data where edges, middle bars, and whiskers indicated 25^{th} and 75^{th} percentiles, median, 5^{th} and 95^{th} percentiles, respectively. One-way analysis of variance (ANOVA) with post-hoc Tukey's test was used to assess the statistical difference among samples using OriginPro 8.6 software. *p value lower than 0.05 was considered statistically significant.

3. Results and discussion

3.1. Fiber Scaffold Fabrication and Characterization

To test our hypothesis (Fig. 1a–c) using biomimetic and estrogenic fiber scaffolds to promote skin repair via the ER-β pathway, we produced ECM-mimetic HA/SPI composite fibers using immersion Rotary Jet Spinning (iRJS, Fig. 1d and Fig. S1a–f). The iRJS is a dryjet wet spinning platform that uses centrifugal forces to drive jet elongation and

coagulation solutions to form fibers from precursor water-based solvents, which is often not compatible with other fiber manufacturing platforms [19–21]. Moreover, our system has a higher production rate (10 mL/min) than traditional electrospinning systems (< 1mL/min) [37, 38]. Here, HA was utilized as a carrier polymer for the genistein-bearing SPI since HA is a water-soluble glycosaminoglycan that forms meshed networks in the native skin microenvironment [19]. Because phytoestrogens are only slightly soluble in pure water, the HA and SPI composite were prepared in water/dimethyl sulfoxide (DMSO) (6:1) to fully dissolve soy phytoestrogens prior to the spinning processes [39, 40]. The concentration of SPI (0, 2, and 4%, wt/v) was varied to identify an optimal concentration for continuous and bead-free fibers with a fixed concentration of the HA backbone (2% wt/v). Pure HA (2% wt/v) and HA/SPI (2%/2% wt/v) solutions exhibited bead-free microfibers (Fig. 1e and f), whereas HA/SPI (2%/4% wt/v) solutions showed beading in the microfibers (Fig. S1b). The rheological measurements confirmed that pure HA (2% wt/v) and HA/SPI (2%/2% wt/v) dopes exhibited shear thinning behaviors, which in turn prevented beading or fiber breakage (Fig. S2) [41]. Accordingly, for further characterization and assessment, we used HA/SPI (2%/2% wt/v) fibers as our sample and pure HA (2% wt/v) fibers as a control. The spun microfibers were composed of nanofibrils whose diameters were ~10 nm (Fig. S1c and d), thus mimicking to some degree the multiscale architecture of collagen fibers in the native skin microenvironment [42, 43]. However, the spun fibers quickly dissolved in a physiological medium (such as phosphate-buffered saline (PBS)) due to the non-covalent nature of bonds between the molecular building blocks of the scaffolds. To address this instability, the fibers were crosslinked using 1-ethyl-3-(3-dimethylaminopropyl) carbodiimide (EDC) and *N*-hydroxysuccinimide (NHS) [44]. The biomimetic fibrillar structure was also preserved in the crosslinked fibers (Fig. 1g and h and Fig. S1e and f). When tested in PBS at 37 °C (Fig. 1i), the crosslinked HA/SPI fibers gradually degraded over 5 days, through hydrolysis of HA and SPI as previously described [23, 45], thus confirming the improved biostability of the scaffolds. In the presence of hyaluronidase, significant mass loss (52 %) of the scaffolds was observed after 1 hour of enzyme treatment and complete degradation of the scaffolds occurred after 1 day (Fig S3).

We also performed energy-dispersive X-ray spectroscopy (EDS) to confirm the removal of DMSO from the scaffold (Fig. S4). There was only negligible noise in the sulfur mapping (S K), suggesting that DMSO is properly removed after fiber fabrication and crosslinking processes. Moreover, the swelling property of the scaffolds was measured to test their water absorption capability (Fig. S5). Both HA and HA/SPI scaffolds showed high water absorption within a day (higher than 2000 %) of swelling, similar to commercial absorbent dressings (such as hydrocolloids) [46]. After 4 days of swelling, they reached a plateau at a higher absorption of 3000 ~ 4000 %. We further performed an in vitro cytotoxicity assay based on lactate dehydrogenase (LDH), a marker for tissue necrosis, to assess the cytocompatibility of the scaffolds. When cultured with human dermal fibroblasts *in vitro* (Fig. S6), LDH data revealed no apparent toxicity and no significant difference were measured between controls (healthy cells cultured in a cell culture dish) and our scaffolds. Collectively, the iRJS platform along with EDC/NHS crosslinking enabled to produce nanofibrous and cytocompatible fiber scaffolds.

We further characterized the structural properties of the engineered fiber scaffolds to study the effects of the addition of SPI to the HA backbone and EDC/NHS crosslinking on fiber diameter, porosity, and mechanical strength. These parameters are known to be crucial for expediting wound healing [47, 48]. First, fiber diameters increased after the crosslinking reaction, whereas the addition of SPI to the fibers barely influenced the fiber diameter (Fig. S7a). In all cases, fiber diameters ranged from 1 to 3 μm, similar to that of *in vivo* collagen microfibrils [42]. Regardless of the presence of SPI and the use of the crosslinker, the engineered scaffolds possessed a highly porous architecture (> 50% porosity, Fig. S7b) that could promote cell infiltration and growth [48]. The Young's moduli of the scaffolds increased after crosslinking and slightly decreased after the addition of SPI (Fig. S7c), which is consistent with our previous observation [23]. Moreover, the Young's moduli of the scaffolds are between 1 and 10 kPa, similar to that of healthy human dermis [49]. Due to the favorable biostability and structural cues, the crosslinked HA and HA/SPI fiber scaffolds were used as our control and test sample, respectively, in the following studies.

In addition, FT-IR measurements were performed to further characterize scaffold composition and monitor chemical crosslinking (Fig. S7d), as previously reported [50, 51]. The EDC/NHS reagent enabled the formation of ester bonds from carboxylic groups and hydroxyl groups (between HA-HA, HA-SPI, or SPI-SPI) and amide bonds from carboxylic groups and amine groups (between HA-SPI or SPI-SPI) [52]. The increase in peaks specific to C=O of esters (at 1700–1800 cm^{-1}) and amides (at 1600–1700 cm^{-1}) suggests crosslinking among HA and SPI molecules. In addition, the increase in the amide peak in HA/SPI fiber scaffolds compared to pure HA fiber scaffolds supports that SPI was successfully integrated into the HA backbone. Moreover, the region between 945 and 1200 cm^{-1} is sensitive to the order of the polymer chains which are comprised of coupled C-O, C-C, and COH vibrational modes [53]. Regardless of crosslinking, both HA and HA/SPI fibers exhibited formation of new bands at ~ 946, 1074, and 1150 cm^{-1}, compared to the powder reference. These data demonstrated that our scaffolds possess higher order after spinning, compared to the powder before spinning.

Next, the phytoestrogen content of the composite fiber scaffolds was measured using liquid chromatography–mass spectrometry (LC-MS) (Fig. 1j–l). Specifically, we focused on detecting genistein, which is one of the main soy phytoestrogens known to trigger the ER-β pathway that could enhance skin repair [14–16, 54]. The major peak of the positively ionized genistein molecule was observed at *m/z* 271, with a retention time of 7 min in LC (Fig. 1j and k). This peak was found in raw SPI powder and HA/SPI fiber scaffolds but not in pure HA fiber scaffolds. Furthermore, the genistein and HA release profile of the HA/SPI fiber scaffolds was analyzed under physiologically relevant conditions by submerging the scaffolds in PBS at 37 °C (Fig. 1l and Fig. S8 and S9). Genistein and HA were gradually released from the scaffolds over 5 days (Fig. 1l and Fig. S9a), followed by first-order release kinetics (Fig. S8 and S9b) [55]. At 5 days of incubation, the scaffolds were almost completely degraded, exhibiting 92.7% genistein and 100% HA release. In addition to scaffold degradation, passive diffusion of genistein may also contribute to the molecule release due to the high surface area of nanofibers [56]. We also measured the ER-β binding affinity of HA/SPI dope and the components released from HA/SPI scaffolds (Fig. S10) using a commercial binding assay kit [57]. We used 17-β-estradiol, which is known to bind

to ER-β in our body [1], as a control to verify the binding assay. 17-β-estradiol exhibited EC_{50} of 0.198 nM (or 53.9 ng/L). The HA/SPI dope and released components from scaffolds both showed a sigmoidal dose-response curve (EC_{50}=2.33 μg/mL for HA/SPI dope and 56.41 μg/mL for HA/SPI scaffolds), confirming the ER-β binding affinity. Altogether, these data suggest that HA/SPI scaffolds can deliver genistein locally to trigger ER-β signaling pathways at the wound site.

3.2. Enhanced Skin Repair in Mice Skin via Estrogen Receptor β

We reasoned that the biomimetic and estrogenic cues from HA/SPI scaffolds will promote skin repair via the ER-β signaling pathways. To test this hypothesis, a full-thickness mouse excisional splinting wound model was utilized (Fig. 2a). All mice underwent ovariectomy surgery (OVX, ovariectomized) and were fed a soy-free diet to hinder endogenous and external sources of estrogen and phytoestrogens other than our scaffolds [8, 10, 14]. The mouse splinting wound model is utilized to better recapitulate the healing processes that occur in humans by re-epithelialization as opposed to the wound contraction observed in non-splinting models [28]. Wound healing experiments with OVX ER-β knock-out (KO) mice were also conducted to study the effects of our scaffolds on cutaneous repair via the ER-β signaling pathway [6, 8]. Each mouse had 6 mm circular cutaneous wounds at day 0, which were then assessed for skin repair at day 20 when all the wounds were fully closed. As a control, wounds that received no treatment were compared to those treated with fibers.

Firstly, ER-β immunostaining was conducted with tissues harvested on day 20 postsurgery in an effort to analyze the expression of the ER-β during wound healing (Fig. 2b and c). Cytokeratin 14 (K14), expressed in epidermal keratinocyte layers and hair follicles, was also immunostained across all samples to visualize skin appendages [58]. As expected, ER-β was highly expressed in the skin appendages of the OVX wild-type (WT) mice (Fig. 2b and Fig. S11), as demonstrated by the overlap between ER-β-positive and K14-positive areas[9]. On the other hand, OVX ER-β KO mice skin only showed non-specific ER-β antibody staining in the cornified layer (Fig. S12), as previously reported [59]. The HA/SPI scaffolds exhibited the highest expression of ER-β in the wound site as compared to control and the HA scaffolds in the OVX WT mice (Fig. 2c). Except for the non-specific staining of the cornified layer, the ER-β expression was not detected in OVX ER-β KO mouse tissues without regard to treatment. Finally, to quantitatively compare ER-β expression among different treatment conditions, we used Skin Tissue Architecture Quality (STAQ) index (Fig. S13). The STAQ index analysis calculates the overlap between healthy and healed skin tissues after 20 days of wound healing. In line with our statistical analysis using one-way analysis of variance (ANOVA) with post-hoc Tukey's test (Fig. 2c), OVX ER-β KO mice showed lower ER-β expression than OVX WT mice. Moreover, a higher expression of ER-β in the wound sites was observed for the HA/SPI scaffolds when compared to controls and HA scaffolds in OVX WT mice. This suggests that the genistein-bearing HA/SPI scaffolds may activate the expression of ER-β in mouse skin that is known to mediate beneficial effects in wound healing.

Next, we measured neo-epidermis length and dermal wound gap (Fig. 3a) as metrics for evaluating how our scaffolds modulated the formation of the epidermal and dermal

layers [33, 34, 60, 61]. The neo-epidermis comprises the newly formed epithelial layers consisting of proliferative and non-differentiated keratinocytes during the early stage of cutaneous healing [60, 61]. Dermal wound gap indicates unresolved granulation tissue without complete regeneration of dermis such as skin appendages [33, 34]. When tissue repair was tested in untreated and scaffold-treated OVX WT mice (Fig. 3b–d), the HA/SPI scaffolds resulted in significantly smaller dermal wound gaps as compared to control and HA scaffolds. Similarly, neo-epidermis length in OVX WT mice was significantly lower in the HA/SPI-treated wounds than control or the HA-treated wounds. When wound healing was measured in untreated and scaffold-treated OVX ER-β KO mice (Fig. 3e–g), regardless of the treatment condition, the dermal wound gap and neo-epidermis length in OVX ER-β KO mice was significantly higher than that in OVX WT mice (Fig. 3h and i). These results demonstrate that the depletion of ER-β causes delayed healing in line with previous studies [8, 15]. Moreover, the beneficial effects of the HA/SPI scaffolds on the dermal tissue repair in OVX WT mice were not observed in OVX ER-β KO mice (Fig. 3h). There was also no significant difference in the dermal wound gap between control, HA-, and HA/SPI-treated wounds in the OVX ER-β KO mice. Likewise, the reduced neo-epidermis by the HA/SPI scaffolds in OVX WT mice was not found in OVX ER-β KO mice (Fig. 3i).

In addition, wound healing tests were also investigated in a normal mouse skin model without ovariectomy to further test whether released genistein and HA-based scaffolds could promote skin tissue repair in normal mice (Fig. S14). Consistent with our *in vivo* results in the OVX mice (Fig. 3), the HA/SPI scaffolds showed significantly smaller dermal wound gaps and neo-epidermis lengths compared to the HA scaffolds or controls. Moreover, dermal wound gaps and neo-epidermis lengths in control wounds were significantly greater than those in wounds treated by the HA scaffolds. Altogether, these *in vivo* data suggest that our HA/SPI scaffolds accelerate epidermal and dermal tissue repair in mouse skin, which involve the ER-β pathway as a major driving mechanism.

3.3 Enhanced Human Skin Repair via Estrogen Receptor β

Although human-mimetic mouse wound healing studies suggested the efficacy of our fibrous soy protein wound dressings, the mouse model does not fully recapitulate the healing in human skin [31]. Therefore, we questioned whether HA/SPI scaffolds could promote tissue repair in a human skin *ex vivo* model, thus implying conservation of the ER-β potency. To test this premise, wound closure in *ex vivo* human skin samples was examined for 7 days (NativeSkin, Fig. 4a–c) [31]. An *ex vivo* human skin biopsy can provide a pre-clinical model for determining human-dependent mechanisms of the healing process using wound dressings [31].

The ER-β signaling pathway was selectively inhibited by an ER-β antagonist (4-[2-phenyl-5,7-bis(trifluoromethyl)pyrazolo[1,5-a]pyrimidin-3-yl]phenol, or PHTPP) to study the effect of the scaffolds on *ex vivo* healing processes via the ER-β [8]. By measuring the distance between the newly formed epidermal layers (called the epithelial gap, Fig. 4d), we investigated the re-epithelialization rate to understand how the engineered materials affect wound closure in human skin. Seven days after the injury, the HA/SPI scaffolds significantly promoted re-epithelialization compared to control and HA scaffolds (Fig.

4e–g). Following treatment with PHTPP that selectively inhibits the ER-β pathway, the re-epithelialization rate by the HA/SPI scaffolds was significantly reduced (Fig. 4h and i). Additionally, to verify the expression of ER-β in the healed skin samples, we performed ER-β immunostaining. Consistent with the *in vivo* results (Fig. 2), human skin treated with the HA/SPI scaffolds had the largest ER-β-positive area among all the conditions (Fig. 4j–l). However, the expression of ER-β in the wound bed and newly formed epithelial tongues was retarded by PHTPP (Fig. 4m). We did not observe any significant difference in re-epithelialization between each donor (Fig. S15), which is consistent with previously published results [62]. Taken together, these results suggest that the HA/SPI scaffolds promote human tissue repair via the ER-β as a major driving mechanism.

4. General discussion and conclusion

Estrogen has been utilized to reverse delayed wound healing in post-menopausal women by stimulating the ER-β pathway [3, 6, 8]. However, the non-preferential binding of this hormone can elicit negative collateral effects, limiting its use for regenerative therapies [11]. To overcome this problem, we hypothesized that the ER-β signaling pathway is the principal mechanism that is activated by the biomimetic and estrogenic soy scaffolds to promote skin repair. To test this hypothesis, we first designed our scaffold to account for the critical role of fibrous dermal ECM architecture in maintaining homeostasis and tissue repair *in vivo* [43, 63, 64]. To this end, our scaffolds were built with water-soluble HA as a carrier polymer during fiber spinning, because HA is an ubiquitous component of the native skin ECM network [65, 66]. Although HA has been integrated in commercial wound dressings as a bioactive component, engineering pure HA nanofibers has been challenging due to low production rates, thick fiber diameters, and nonhomogeneous structures that are associated with the limitations of previous techniques (*e.g.,* electrospinning) [38, 67]. We recently developed a nanofiber manufacturing platform (called iRJS) that allows a high throughput production of HA-based nanofibers [41]. Our scaffolds produced by the original platform successfully recapitulated aspects of multiscale architecture and the fibrous nature of the native skin microenvironment [43]. Due to the fibrous structure and hydrophilic molecules, the scaffolds exhibited highly absorbent capability that can provide a hydrated environment for accelerated wound healing [46]. These implantable and biodegradable scaffolds can be easily applied to wound sites for local delivery of bioactive molecules to accelerate wound healing [43, 68–73].

Genistein, one of the main phytoestrogens endogenous to soy protein, is incorporated as the bioactive compound in our scaffold design [11, 14, 74, 75]. This phytoestrogen serves as a local ER-β modulating molecule for accelerated wound healing [14]. Although genistein has been studied as a selective ER-β modulator, engineering genistein or soy phytoestrogen scaffolds remains poorly explored. Previous reports describing topical and oral administration of genistein, or genistein-bearing soy protein (such as SPI), described enhanced skin repair (wound closure and hair regrowth) in animal models [11, 14, 17, 18, 74–76]. However, sustained administration, either topically or orally, may potentiate maladaptive, negative effects [77]. We reasoned that an alternative strategy, nanofiber scaffolds, would offer controlled, localized release of the therapeutic molecule while mimicking the ECM architecture required for cell migration and proliferation in the wound.

Because previous studies have relied on *in vitro* or *in vivo* models [14, 74–76, 78], there is also a need to investigate the effect of genistein and the ER-β pathway in the context of human skin repair to improve clinical relevance. Moreover, these methods did not control for the release of genistein and for the recapitulation of the physicochemical properties (for instance, a nanofibrous architecture) that are known to support homeostasis and innate healing processes in our body [79]. Some studies did not report that genistein could be loaded within engineered nanofibers [78, 80]. However, these studies used synthetic backbone polymers that can be considered suboptimal materials for wound healing because of their limited biomimetic chemical and structural properties [43, 81, 82]. More importantly, how the delivery of phytoestrogens from nanofibers affects the ER-β signaling pathway for skin repair remained to be determined. It was therefore critical to combine the manufacturing platform, HA nanofibers, and genistein to reveal how these engineered biomimetic and estrogenic fibers influence this ER-β pathway for enhanced skin repair.

To address these issues, we incorporated SPI with biomimetic HA fibrous backbone as an ER-β-triggering genistein source. After the addition of 2% SPI, the scaffolds maintained nanofibrous architecture with homogenous distribution of SPI throughout the scaffolds. Due to the fast dissolution of the HA-based scaffolds in physiological conditions, the scaffolds needed to be chemically crosslinked via EDC/NHS coupling, which is known to have no cytotoxicity when the crosslinked scaffolds are washed thoroughly [83]. The crosslinked scaffold was gradually degraded in PBS over 5 days, indicating improved biostability after crosslinking process. In the presence of hyaluronidase that degrades HA in the native microenvironment, the scaffold was quickly degraded within 1 day due to fast degradation of HA by the enzyme. The *in vitro* degradation rates were much faster than the actual scaffold degradation during *in vivo* and *ex vivo* experiments. The difference in degradation rates results from *in vitro* degradation testing conditions in a large volume of solution, whereas the scaffolds are only exposed to a small volume of solution during *in vivo* and *ex vivo* healing processes. A previous study, which focused on understanding the effect of iRJS-spun HA scaffolds early in the healing process (at day 6), showed us that HA products were still present at that time [41], suggesting similar results should be expected with HA/SPI scaffolds. Additionally, it should be noted that degraded products of HA may play alternating roles in inflammation. For instance, anti-inflammatory and pro-resolving responses were found on high molecular weight HA (over 1 million Da, similar to HA in the native tissues), while pro-inflammatory response was found on low molecular weight HA (lower than 1 million Da) [84–86].

To verify the existence and release of the ER-β-triggering genistein from our scaffolds, we performed LC-MS analysis on dissolved HA/SPI samples. LC-MS data showed the genistein-specific peak (m/z= 271), confirming the presence of genistein in our scaffolds. While being degraded in a physiologically relevant condition (PBS at 37 °C), our scaffolds gradually delivered genistein over 5 days and were fully degraded at day 5. This degradation tendency followed a first-order release kinetics, previously observed for bconcentration-dependent release from porous matrices [87]. Moreover, an ER-β binding assay was conducted to verify the binding affinity of released genistein from HA/SPI scaffolds with ER-β receptor. The EC_{50} of HA/SPI scaffolds (5.641 mg/mL) was higher than that of 17-β-estradiol (0.198 nM or 53.9 ng/L) or genistein (~ 5 nM or ~ 1 μg/L) [88]. It should

be noted that, while only a small amount of 17-β-estradiol or genistein (less than 100 μg) per animal or human (based on their body weights) is needed to trigger the ER-β for accelerating wound healing [5, 6, 14, 74, 76, 89], a few grams of our scaffolds directly applied to the small wound sites allow for a local modulation of ER-β levels. Additionally, our results suggest that HA/SPI scaffolds have lower binding affinity than the HA/SPI dopes. This indicates that some of the ER-β-triggering molecules (such as genistein) were lost during fiber spinning or crosslinking processes. The environment provided by other scaffold components to genistein could have also affected its ER-β binding activity. Nonetheless, sufficient amounts of the active component in HA/SPI were left to enable ER-β binding as confirmed by the sigmoidal dose response curve recorded from the binding assay.

Next, the effect of our scaffold in wound healing and ER-β signaling pathway was investigated in mouse skin. Here, we used a standard OVX female mouse model to study the effect of exogenous estrogenic compounds on wound healing by inhibiting the production of endogenous estrogen [1, 5, 6]. OVX female mice display indeed a delayed healing response compared to normal female mice due to the lack of endogenous estrogen [6]. However, when OVX female mice are treated with estrogen or genistein, the delayed healing is reversed [6, 90]. In our study, wound healing control tests in OVX ER-β KO female mice were thus performed to verify whether our scaffolds could trigger the ER-β pathway during wound healing [1, 5, 6]. We performed our *in vivo* experiments with female mice because the effect of our scaffolds on wound healing and ER-β signaling may vary in male mice, considering their differences in estrogen expression, physiology, and pathology [89, 91]. We also designed *in vivo* experiments to investigate outcomes (dermal and epidermal tissue repair) at a later stage (day 20) of wound healing, to allow comparison with recent wound healing studies [92–94].

Consequently, our ER-β immunostaining data indicates that the OVX ER-β KO mice had no significant ER-β expression regardless of treatment except for the non-specific staining of the cornified layers. On the other hand, HA/SPI-treated OVX WT mice exhibited higher ER-β expression compared to HA-treated or control wounds. The higher ER-β expression by HA/SPI scaffolds was further confirmed by a quantitative statistic assessment (STAQ) index) [35, 36]. These results are in line with previous studies where genistein was topically or orally provided [14, 74–76], supporting that the genistein-bearing scaffolds can trigger the ER-β signaling pathway in mouse skin. HA-treated wounds exhibited a higher ER-β expression than control wounds. One possible explanation is that HA-treated wounds had a higher non-specific ER-β antibody staining in the cornified layer and thus higher ER β-positive area compared to control wounds in OVX WT mice. On the other hand, HA/SPI-treated wounds showed higher ER β-positive area not only in the outmost epithelial layer, but also in the dermal layer. Our wound healing study in normal mice without ovariectomy further supports that HA-based fibrous backbone can accelerate skin tissue repair in normal mice regardless of the ER-β signaling. Furthermore, HA/SPI scaffolds outperformed controls (no treatment or HA only scaffolds) in dermal and epidermal tissue repair in both OVX WT and normal (without ovariectomy surgery) mice, but not in OVX ER-β KO mice in which the ER-β pathway is inhibited. Altogether, these *in vivo* data suggest that HA/SPI scaffolds may activate the ER-β and in turn, accelerate tissue repair.

Although our current and previous *in vivo* studies provide crucial insights on the ER-β-mediated skin repair by soy phytoestrogen in animal models, the influence of genistein within engineered scaffolds on wound healing via the ER-β in human skin still remains unexplored. To address this limitation, we performed wound healing studies based on an *ex vivo* human skin model donated from female patients. To investigate the healing process at an earlier timepoint, we performed ex vivo wound healing experiments with human skin to examine results within a week (day 7). In line with our *in vivo* mouse data, HA/SPI scaffolds exhibited faster re-epithelialization than control (no treatment) or HA only scaffolds. To test whether the accelerated re-epithelialization was achieved via the ER-β pathway or not, we added an ER-β selective antagonist (PHTPP) to HA/SPI-treated wounds. Once PHTPP was applied, HA/SPI scaffolds were not able to promote re-epithelialization, but the re-epithelialization rates of untreated control or HA-treated samples were similar. On top of that, the ER-β expression triggered by HA/SPI scaffold was also inhibited when treated with PHTPP. To the best of our knowledge, our *ex vivo* study revealed, for the first time, that genistein-bearing scaffolds can accelerate wound healing in human skin tissue via the ER-β pathway. In summary, our findings suggest that the genistein delivery and fibrous nature of our HA/SPI scaffolds enable accelerated cutaneous repair in both mouse and human skin via the ER-β pathway.

Supplementary Material

Refer to Web version on PubMed Central for supplementary material.

Acknowledgements

This research was performed in part at the Center for Nanoscale Systems (CNS), a member of the National Nanotechnology Infrastructure Network (NNIN), which is supported by the National Science Foundation under NSF award no. 1541959. CNS is part of Harvard University. This study was partly supported by the Harvard University Materials Research Science and Engineering Center (MRSEC), NSF Award No. DMR-1420570. We thank Dana-Farber/Harvard Cancer Center in Boston, MA, for the use of the Specialized Histopathology Core, which provided tissue preparation and histology staining services. Dana-Farber/Harvard Cancer Center is supported in part by an NCI Cancer Center Support Grant # NIH 5 P30 CA06516. We thank the Neurobiology Department and the Neurobiology Imaging Facility for consultation and instrument availability that supported this work. This facility is supported in part by the Neural Imaging Center as part of an NINDS P30 Core Center grant #NS072030. H. A. M. A. would like to thank the American Chemical Society for generous support through the Irving S. Sigal Postdoctoral Fellowship. The authors appreciate the graphic works provided by Su-Yeon Choi and Michael Rosnach.

Data availability

The data generated during the current study are available from the corresponding author on reasonable request.

References

[1]. Hall G, Phillips TJ, Estrogen and skin: the effects of estrogen, menopause, and hormone replacement therapy on the skin, J. Am. Acad. Dermatol 53(4) (2005) 555–568. [PubMed: 16198774]

[2]. Brisken C, Progesterone signalling in breast cancer: a neglected hormone coming into the limelight, Nat. Rev. Cancer 13(6) (2013) 385. [PubMed: 23702927]

[3]. Lopez MM, Castillo AC, Kaltwasser K, Phillips LG, Moliver CL, Surgical timing and the menstrual cycle affect wound healing in young breast reduction patients, Plast. Reconstr. Surg 137(2) (2016) 406–410. [PubMed: 26818273]

[4]. LeBlanc ES, Janowsky J, Chan BK, Nelson HD, Hormone replacement therapy and cognition: systematic review and meta-analysis, Jama 285(11) (2001) 1489–1499. [PubMed: 11255426]

[5]. Ashcroft GS, Greenwell-Wild T, Horan MA, Wahl SM, Ferguson MW, Topical estrogen accelerates cutaneous wound healing in aged humans associated with an altered inflammatory response, Am J Pathol 155(4) (1999) 1137–1146. [PubMed: 10514397]

[6]. Ashcroft GS, Dodsworth J, vAN BoxTEL E, Tarnuzzer RW, Horan MA, Schultz GS, Ferguson MW, Estrogen accelerates cutaneous wound healing associated with an increase in TGF-β1 levels, Nat. Med 3(11) (1997) 1209–1215. [PubMed: 9359694]

[7]. Dahlman-Wright K, Cavailles V, Fuqua SA, Jordan VC, Katzenellenbogen JA, Korach KS, Maggi A, Muramatsu M, Parker MG, Gustafsson J-Å, International union of pharmacology. LXIV. Estrogen receptors, Pharmacol. Rev 58(4) (2006) 773–781. [PubMed: 17132854]

[8]. Campbell L, Emmerson E, Davies F, Gilliver SC, Krust A, Chambon P, Ashcroft GS, Hardman MJ, Estrogen promotes cutaneous wound healing via estrogen receptor β independent of its antiinflammatory activities, J. Exp. Med 207(9) (2010) 1825–1833. [PubMed: 20733032]

[9]. Ohata C, Tadokoro T, Itami S, Expression of estrogen receptor β in normal skin, melanocytic nevi and malignant melanomas, J. Dermatol 35(4) (2008) 215–221. [PubMed: 18419678]

[10]. Hardman MJ, Emmerson E, Campbell L, Ashcroft GS, Selective estrogen receptor modulators accelerate cutaneous wound healing in ovariectomized female mice, Endocrinology 149(2) (2007) 551–557. [PubMed: 17974625]

[11]. Irrera N, Pizzino G, D'Anna R, Vaccaro M, Arcoraci V, Squadrito F, Altavilla D, Bitto A, Dietary management of skin health: the role of genistein, Nutrients 9(6) (2017) 622. [PubMed: 28629129]

[12]. Han SJ, Begum K, Foulds CE, Hamilton RA, Bailey S, Malovannaya A, Chan D, Qin J, O'Malley BW, The dual estrogen receptor α inhibitory effects of the tissue-selective estrogen complex for endometrial and breast safety, Mol. Pharmacol 89(1) (2016) 14–26. [PubMed: 26487511]

[13]. Sacks FM, Lichtenstein A, Van Horn L, Harris W, Kris-Etherton P, Winston M, Soy protein, isoflavones, and cardiovascular health, Circulation 113(7) (2006) 1034–1044. [PubMed: 16418439]

[14]. Emmerson E, Campbell L, Ashcroft GS, Hardman MJ, The phytoestrogen genistein promotes wound healing by multiple independent mechanisms, Mol. Cell. Endocrinol 321(2) (2010) 184–193. [PubMed: 20193736]

[15]. Kuiper GG, Lemmen JG, Carlsson B, Corton JC, Safe SH, Van Der Saag PT, Van Der Burg B, J.-A.k. Gustafsson, Interaction of estrogenic chemicals and phytoestrogens with estrogen receptor β, Endocrinology 139(10) (1998) 4252–4263. [PubMed: 9751507]

[16]. Harada N, Okajima K, Arai M, Kurihara H, Nakagata N, Administration of capsaicin and isoflavone promotes hair growth by increasing insulin-like growth factor-I production in mice and in humans with alopecia, Growth Horm. IGF Res 17(5) (2007) 408–415. [PubMed: 17569567]

[17]. Shevchenko RV, Santin M, Pre-clinical evaluation of soybean-based wound dressings and dermal substitute formulations in pig healing and non-healing in vivo models, Burns Trauma 2(4) (2014) 187. [PubMed: 27602381]

[18]. Babajafari S, Akhlaghi M, Mazloomi SM, Ayaz M, Noorafshan A, Jafari P, Hojhabrimanesh A, The effect of isolated soy protein adjunctive with flaxseed oil on markers of inflammation, oxidative stress, acute phase proteins, and wound healing of burn patients; a randomized clinical trial, Burns (2017).

[19]. Pashuck ET, Stevens MM, Designing regenerative biomaterial therapies for the clinic, Sci. Transl. Med 4(160) (2012) 160sr4–160sr4.

[20]. Lohmann N, Schirmer L, Atallah P, Wandel E, Ferrer RA, Werner C, Simon JC, Franz S, Freudenberg U, Glycosaminoglycan-based hydrogels capture inflammatory chemokines and rescue defective wound healing in mice, Sci. Transl. Med 9(386) (2017) eaai9044.

[21]. Gonzalez GM, MacQueen LA, Lind JU, Fitzgibbons SA, Chantre CO, Huggler I, Golecki HM, Goss JA, Parker KK, Production of Synthetic, Para-Aramid and Biopolymer Nanofibers by Immersion Rotary Jet-Spinning, Macromol. Mater. Eng 302(1) (2017).

[22]. Hotaling NA, Bharti K, Kriel H, Simon CG, DiameterJ: A validated open source nanofiber diameter measurement tool, Biomaterials 61 (2015) 327–338. [PubMed: 26043061]

[23]. Ahn S, Chantre CO, Gannon AR, Lind JU, Campbell PH, Grevesse T, O'Connor BB, Parker KK, Soy Protein/Cellulose Nanofiber Scaffolds Mimicking Skin Extracellular Matrix for Enhanced Wound Healing, Adv. Healthcare Mater 7(9) (2018) e1701175.

[24]. Shah DN, Recktenwall-Work SM, Anseth KS, The effect of bioactive hydrogels on the secretion of extracellular matrix molecules by valvular interstitial cells, Biomaterials 29(13) (2008) 2060–2072. [PubMed: 18237775]

[25]. Malaisse J, Pendaries V, Hontoir F, De Glas V, Van Vlaender D, Simon M, de Rouvroit CL, Poumay Y, Flamion B, Hyaluronan does not regulate human epidermal keratinocyte proliferation and differentiation, J. Biol. Chem 291(12) (2016) 6347–6358. [PubMed: 26627828]

[26]. Chan FK-M, Moriwaki K, De Rosa MJ, Detection of necrosis by release of lactate dehydrogenase activity, Methods Mol. Biol (2013) 65–70.

[27]. Zhang J-H, Chung TD, Oldenburg KR, A simple statistical parameter for use in evaluation and validation of high throughput screening assays, J. Biomol. Screen 4(2) (1999) 67–73. [PubMed: 10838414]

[28]. Wang X, Ge J, Tredget EE, Wu Y, The mouse excisional wound splinting model, including applications for stem cell transplantation, Nat. Protoc 8(2) (2013) 302. [PubMed: 23329003]

[29]. Charan J, Kantharia N, How to calculate sample size in animal studies?, Journal of pharmacology & pharmacotherapeutics 4(4) (2013) 303. [PubMed: 24250214]

[30]. Faul F, Erdfelder E, Lang A-G, Buchner A, G* Power 3: A flexible statistical power analysis program for the social, behavioral, and biomedical sciences, Behavior research methods 39(2) (2007) 175–191. [PubMed: 17695343]

[31]. De Wever B, Kurdykowski S, Descargues P, Human skin models for research applications in pharmacology and toxicology: Introducing NativeSkin®, the "missing link" bridging cell culture and/or reconstructed skin models and human clinical testing, Applied In Vitro Toxicology 1(1) (2015) 26–32.

[32]. Emmerson E, Campbell L, Davies FC, Ross NL, Ashcroft GS, Krust A, Chambon P, Hardman MJ, Insulin-like growth factor-1 promotes wound healing in estrogen-deprived mice: new insights into cutaneous IGF-1R/ERα cross talk, J. Investig. Dermatol 132(12) (2012) 2838–2848. [PubMed: 22810305]

[33]. Kwon YW, Heo SC, Lee TW, Park GT, Yoon JW, Jang IH, Kim S-C, Ko H-C, Ryu Y, Kang H, N-acetylated proline-glycine-proline accelerates cutaneous wound healing and neovascularization by human endothelial progenitor cells, Scientific reports 7 (2017) 43057. [PubMed: 28230162]

[34]. Rønø B, Engelholm LH, Lund LR, Hald A, Gender affects skin wound healing in plasminogen deficient mice, PloS one 8(3) (2013) e59942.

[35]. Chantre CO, Campbell PH, Golecki HM, Buganza AT, Capulli AK, Deravi LF, Dauth S, Sheehy SP, Paten JA, Gledhill K, Production-scale fibronectin nanofibers promote wound closure and tissue repair in a dermal mouse model, Biomaterials 166 (2018) 96–108. [PubMed: 29549768]

[36]. Ahn S, Ardoña HAM, Campbell PH, Gonzalez GM, Parker KK, Alfalfa Nanofibers for Dermal Wound Healing, ACS Appl. Mater. Interfaces 11(37) (2019) 33535–33547. [PubMed: 31369233]

[37]. Um IC, Fang D, Hsiao BS, Okamoto A, Chu B, Electro-spinning and electro-blowing of hyaluronic acid, Biomacromolecules 5(4) (2004) 1428–1436. [PubMed: 15244461]

[38]. Uppal R, Ramaswamy GN, Arnold C, Goodband R, Wang Y, Hyaluronic acid nanofiber wound dressing—production, characterization, and in vivo behavior, J. Biomed. Mater. Res., Part B 97(1) (2011) 20–29.

[39]. Wu J-G, Ge J, Zhang Y-P, Yu Y, Zhang X-Y, Solubility of genistein in water, methanol, ethanol, propan-2-ol, 1-butanol, and ethyl acetate from (280 to 333) K, J. Chem. Eng. Data 55(11) (2010) 5286–5288.

[40]. Huang J, Nasr M, Kim Y, Matthews H, Genistein inhibits protein histidine kinase, J. Biol. Chem 267(22) (1992) 15511–15515. [PubMed: 1639791]

[41]. Chantre CO, Gonzalez GM, Ahn S, Cera L, Campbell PH, Hoerstrup SP, Parker KK, Porous Biomimetic Hyaluronic Acid and Extracellular Matrix Protein Nanofiber Scaffolds for Accelerated Cutaneous Tissue Repair, ACS Appl. Mater. Interfaces 11(49) (2019) 45498–45510. [PubMed: 31755704]

[42]. Kadler KE, Holmes DF, Trotter JA, Chapman JA, Collagen fibril formation, Biochem. J 316(1) (1996) 1–11. [PubMed: 8645190]

[43]. Chantre CO, Hoerstrup SP, Parker KK, Engineering Biomimetic and Instructive Materials for Wound Healing and Regeneration, Current Opinion in Biomedical Engineering 10 (2019) 97–106.

[44]. Segura T, Anderson BC, Chung PH, Webber RE, Shull KR, Shea LD, Crosslinked hyaluronic acid hydrogels: a strategy to functionalize and pattern, Biomaterials 26(4) (2005) 359–371. [PubMed: 15275810]

[45]. Patterson J, Siew R, Herring SW, Lin AS, Guldberg R, Stayton PS, Hyaluronic acid hydrogels with controlled degradation properties for oriented bone regeneration, Biomaterials 31(26) (2010) 6772–6781. [PubMed: 20573393]

[46]. Hasatsri S, Pitiratanaworanat A, Swangwit S, Boochakul C, Tragoonsupachai C, Comparison of the morphological and physical properties of different absorbent wound dressings, Dermatology research and practice 2018 (2018).

[47]. Discher DE, Janmey P, Wang Y.-l., Tissue cells feel and respond to the stiffness of their substrate, Science 310(5751) (2005) 1139–1143. [PubMed: 16293750]

[48]. Lowery JL, Datta N, Rutledge GC, Effect of fiber diameter, pore size and seeding method on growth of human dermal fibroblasts in electrospun poly (ε-caprolactone) fibrous mats, Biomaterials 31(3) (2010) 491–504. [PubMed: 19822363]

[49]. Liang X, Boppart SA, Biomechanical properties of in vivo human skin from dynamic optical coherence elastography, IEEE Trans. Biomed. Eng 57(4) (2010) 953–959. [PubMed: 19822464]

[50]. Badrossamay MR, Balachandran K, Capulli AK, Golecki HM, Agarwal A, Goss JA, Kim H, Shin K, Parker KK, Engineering hybrid polymer-protein super-aligned nanofibers via rotary jet spinning, Biomaterials 35(10) (2014) 3188–3197. [PubMed: 24456606]

[51]. Capulli AK, Emmert MY, Pasqualini FS, Kehl D, Caliskan E, Lind JU, Sheehy SP, Park SJ, Ahn S, Weber B, JetValve: Rapid manufacturing of biohybrid scaffolds for biomimetic heart valve replacement, Biomaterials 133 (2017) 229–241. [PubMed: 28445803]

[52]. Grabarek Z, Gergely J, Zero-length crosslinking procedure with the use of active esters, Anal. Biochem 185(1) (1990) 131–135. [PubMed: 2344038]

[53]. Gilli R, Kacuráková M, Mathlouthi M, Navarini L, Paoletti S, FTIR studies of sodium hyaluronate and its oligomers in the amorphous solid phase and in aqueous solution, Carbohydr. Res 263(2) (1994) 315–326. [PubMed: 7805057]

[54]. Zhao J, Harada N, Kurihara H, Nakagata N, Okajima K, Dietary isoflavone increases insulin-like growth factor-I production, thereby promoting hair growth in mice, J. Nutr. Biochem 22(3) (2011) 227–233. [PubMed: 20576422]

[55]. Huang L-Y, Branford-White C, Shen X-X, Yu D-G, Zhu L-M, Time-engineeringed biphasic drug release by electrospun nanofiber meshes, Int. J. Pharm 436(1–2) (2012) 88–96. [PubMed: 22789913]

[56]. Taepaiboon P, Rungsardthong U, Supaphol P, Drug-loaded electrospun mats of poly (vinyl alcohol) fibres and their release characteristics of four model drugs, Nanotechnology 17(9) (2006) 2317.

[57]. Hanson AM, Perera KIS, Kim J, Pandey RK, Sweeney N, Lu X, Imhoff A, Mackinnon AC, Wargolet AJ, Van Hart RM, A–C Estrogens as Potent and Selective Estrogen Receptor-Beta Agonists (SERBAs) to Enhance Memory Consolidation under Low-Estrogen Conditions, J. Med. Chem 61(11) (2018) 4720–4738. [PubMed: 29741891]

[58]. Nijhof JG, Braun KM, Giangreco A, van Pelt C, Kawamoto H, Boyd RL, Willemze R, Mullenders LH, Watt FM, de Gruijl FR, The cell-surface marker MTS24 identifies a novel population of follicular keratinocytes with characteristics of progenitor cells, Development 133(15) (2006) 3027–3037. [PubMed: 16818453]

[59]. Sevilla LM, Nachat R, Groot KR, Klement JF, Uitto J, Djian P, Määttä A, Watt FM, Mice deficient in involucrin, envoplakin, and periplakin have a defective epidermal barrier, J. Cell Biol 179(7) (2007) 1599–1612. [PubMed: 18166659]

[60]. Florin L, Knebel J, Zigrino P, Vonderstrass B, Mauch C, Schorpp-Kistner M, Szabowski A, Angel P, Delayed wound healing and epidermal hyperproliferation in mice lacking JunB in the skin, J. Investig. Dermatol 126(4) (2006) 902–911. [PubMed: 16439969]

[61]. Tscharntke M, Pofahl R, Chrostek-Grashoff A, Smyth N, Niessen C, Niemann C, Hartwig B, Herzog V, Klein HW, Krieg T, Impaired epidermal wound healing in vivo upon inhibition or deletion of Rac1, J. Cell Sci 120(8) (2007) 1480–1490. [PubMed: 17389689]

[62]. Boekema B, Ulrich MMW, Middelkoop E, Models for cutaneous wound healing, Wound Repair Regen 25(2) (2017) 347–348. [PubMed: 28520212]

[63]. Martin P, Wound healing--aiming for perfect skin regeneration, Science 276(5309) (1997) 75–81. [PubMed: 9082989]

[64]. Leung V, Hartwell R, Yang H, Ghahary A, Ko F, Bioactive nanofibres for wound healing applications, J Fiber Bioeng Informat 4 (2011) 1–14.

[65]. Schaefer L, Schaefer RM, Proteoglycans: from structural compounds to signaling molecules, Cell Tissue Res. 339(1) (2010) 237. [PubMed: 19513755]

[66]. Frantz C, Stewart KM, Weaver VM, The extracellular matrix at a glance, J. Cell Sci 123(24) (2010) 4195–4200. [PubMed: 21123617]

[67]. Khorshidi S, Solouk A, Mirzadeh H, Mazinani S, Lagaron JM, Sharifi S, Ramakrishna S, A review of key challenges of electrospun scaffolds for tissue-engineering applications, J. Tissue. Eng. Regen. Med 10(9) (2016) 715–738.

[68]. Boateng JS, Matthews KH, Stevens HN, Eccleston GM, Wound healing dressings and drug delivery systems: a review, J. Pharm. Sci 97(8) (2008) 2892–2923. [PubMed: 17963217]

[69]. Zhao X, Wu H, Guo B, Dong R, Qiu Y, Ma PX, Antibacterial anti-oxidant electroactive injectable hydrogel as self-healing wound dressing with hemostasis and adhesiveness for cutaneous wound healing, Biomaterials 122 (2017) 34–47. [PubMed: 28107663]

[70]. Qu J, Zhao X, Liang Y, Zhang T, Ma PX, Guo B, Antibacterial adhesive injectable hydrogels with rapid self-healing, extensibility and compressibility as wound dressing for joints skin wound healing, Biomaterials 183 (2018) 185–199. [PubMed: 30172244]

[71]. Li M, Chen J, Shi M, Zhang H, Ma PX, Guo B, Electroactive anti-oxidant polyurethane elastomers with shape memory property as non-adherent wound dressing to enhance wound healing, Chem. Eng. J 375 (2019) 121999.

[72]. Liang Y, Zhao X, Hu T, Chen B, Yin Z, Ma PX, Guo B, Adhesive hemostatic conducting injectable composite hydrogels with sustained drug release and photothermal antibacterial activity to promote full-thickness skin regeneration during wound healing, Small 15(12) (2019) 1900046.

[73]. Qu J, Zhao X, Liang Y, Xu Y, Ma PX, Guo B, Degradable conductive injectable hydrogels as novel antibacterial, anti-oxidant wound dressings for wound healing, Chem. Eng. J 362 (2019) 548–560.

[74]. Marini H, Polito F, Altavilla D, Irrera N, Minutoli L, Calo M, Adamo E, Vaccaro M, Squadrito F, Bitto A, Genistein aglycone improves skin repair in an incisional model of wound healing: a comparison with raloxifene and oestradiol in ovariectomized rats, Br. J. Pharmacol 160(5) (2010) 1185–1194. [PubMed: 20590611]

[75]. Tie L, An Y, Han J, Xiao Y, Xiaokaiti Y, Fan S, Liu S, Chen AF, Li X, Genistein accelerates refractory wound healing by suppressing superoxide and FoxO1/iNOS pathway in type 1 diabetes, J. Nutr. Biochem 24(1) (2013) 88–96. [PubMed: 22819564]

[76]. Park E, Lee SM, Jung I-K, Lim Y, Kim J-H, Effects of genistein on early-stage cutaneous wound healing, Biochem. Biophys. Res. Commun 410(3) (2011) 514–519. [PubMed: 21679688]

[77]. Heunis T, Dicks L, Nanofibers offer alternative ways to the treatment of skin infections, BioMed Research International 2010 (2010).

[78]. Buddhiranon S, DeFine LA, Alexander TS, Kyu T, Genistein-modified poly (ethylene oxide)/ poly (d, l-lactic acid) electrospun mats with improved antioxidant and anti-inflammatory properties, Biomacromolecules 14(5) (2013) 1423–1433. [PubMed: 23594342]

[79]. Rieger KA, Birch NP, Schiffman JD, Designing electrospun nanofiber mats to promote wound healing–a review, J. Mater. Chem. B 1(36) (2013) 4531–4541. [PubMed: 32261196]

[80]. Ibrahim S, Sayed HM, El-Rafei A, El Amir A, Ismail M, Allam NK, Improved genistein loading and release on electrospun chitosan nanofiber blends, J. Mol. Liq 223 (2016) 1056–1061.

[81]. Kumbar S, James R, Nukavarapu S, Laurencin C, Electrospun nanofiber scaffolds: engineering soft tissues, Biomed. Mater 3(3) (2008) 034002.

[82]. Place ES, George JH, Williams CK, Stevens MM, Synthetic polymer scaffolds for tissue engineering, Chem. Soc. Rev 38(4) (2009) 1139–1151. [PubMed: 19421585]

[83]. Ahmad Z, Shepherd JH, Shepherd DV, Ghose S, Kew SJ, Cameron RE, Best SM, Brooks RA, Wardale J, Rushton N, Effect of 1-ethyl-3-(3-dimethylaminopropyl) carbodiimide and N-hydroxysuccinimide concentrations on the mechanical and biological characteristics of cross-linked collagen fibres for tendon repair, Regenerative biomaterials 2(2) (2015) 77–85. [PubMed: 26816633]

[84]. Cyphert JM, Trempus CS, Garantziotis S, Size matters: molecular weight specificity of hyaluronan effects in cell biology, International journal of cell biology 2015 (2015).

[85]. Rayahin JE, Buhrman JS, Zhang Y, Koh TJ, Gemeinhart RA, High and low molecular weight hyaluronic acid differentially influence macrophage activation, ACS biomaterials science & engineering 1(7) (2015) 481–493. [PubMed: 26280020]

[86]. Chistyakov DV, Astakhova AA, Azbukina NV, Goriainov SV, Chistyakov VV, Sergeeva MG, High and Low Molecular Weight Hyaluronic Acid Differentially Influences Oxylipins Synthesis in Course of Neuroinflammation, International journal of molecular sciences 20(16) (2019) 3894. [PubMed: 31405034]

[87]. Pisani S, Dorati R, Chiesa E, Genta I, Modena T, Bruni G, Grisoli P, Conti B, Release Profile of Gentamicin Sulfate from Polylactide-co-Polycaprolactone Electrospun Nanofiber Matrices, Pharmaceutics 11(4) (2019) 161. [PubMed: 30987212]

[88]. An J, Tzagarakis-Foster C, Scharschmidt TC, Lomri N, Leitman DC, Estrogen receptor β-selective transcriptional activity and recruitment of coregulators by phytoestrogens, J. Biol. Chem 276(21) (2001) 17808–17814. [PubMed: 11279159]

[89]. Gilliver SC, Emmerson E, Campbell L, Chambon P, Hardman MJ, Ashcroft GS, 17β-Estradiol inhibits wound healing in male mice via estrogen receptor-α, Am J Pathol 176(6) (2010) 2707–2721. [PubMed: 20448060]

[90]. Setchell KD, Soy isoflavones—benefits and risks from nature's selective estrogen receptor modulators (SERMs), J. Am. Coll. Nutr 20(sup5) (2001) 354S–362S. [PubMed: 11603644]

[91]. Nelson LR, Bulun SE, Estrogen production and action, J. Am. Acad. Dermatol 45(3) (2001) S116–S124. [PubMed: 11511861]

[92]. Wu H, Li F, Wang S, Lu J, Li J, Du Y, Sun X, Chen X, Gao J, Ling D, Ceria nanocrystals decorated mesoporous silica nanoparticle based ROS-scavenging tissue adhesive for highly efficient regenerative wound healing, Biomaterials 151 (2018) 66–77. [PubMed: 29078200]

[93]. Muhamed I, Sproul EP, Ligler FS, Brown AC, Fibrin Nanoparticles Coupled with Keratinocyte Growth Factor Enhance the Dermal Wound-Healing Rate, ACS Appl. Mater. Interfaces 11(4) (2019) 3771–3780. [PubMed: 30604611]

[94]. He J, Qiao Y, Zhang H, Zhao J, Li W, Xie T, Zhong D, Wei Q, Hua S, Yu Y, Gold–silver nanoshells promote wound healing from drug-resistant bacteria infection and enable monitoring via surface-enhanced Raman scattering imaging, Biomaterials (2020) 119763.

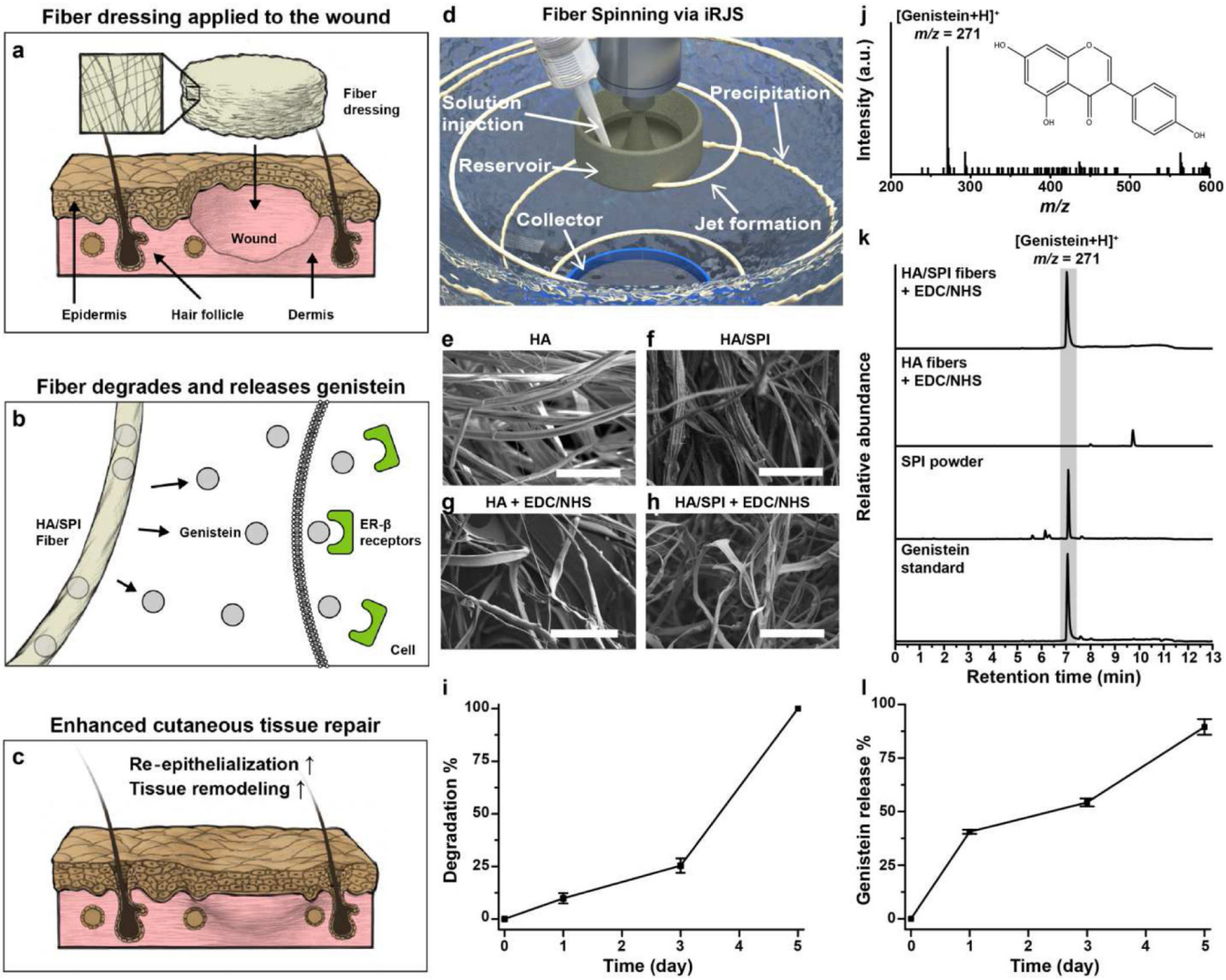

Fig. 1. Fabrication and characterization of genistein-containing fibers.

a–c, Schematic of proposed role of HA/SPI fiber scaffolds for activating the ER-β pathway in cutaneous wounds. (**a**) The engineered scaffolds are locally applied to the wound site. (**b**) During healing processes, the fibers degrade over time and continuously release genistein, an ER-β modulating molecule. The genistein released from the scaffolds binds to the ER-β, (**c**) promoting skin tissue repair. **d**, Schematic of the iRJS machine. **e–h**, SEM images of the engineered fibers. The scales are 50 μm. **i**, Scaffold degradation kinetics were characterized by measuring the weight loss of crosslinked HA/SPI scaffolds in PBS solution. **j–l**, LC-MS analysis of genistein content in scaffolds. (**j**) Full MS spectra of genistein showing the major peak at *m/z* 271 (inset: molecular structure of genistein). (**k**) LC-MS spectra of samples, recorded in SIM mode. The gray area indicates the genistein-specific peaks (retention time: 7 min). (**l**) Genistein release kinetics of crosslinked HA/SPI scaffolds in PBS solution. For statistical analysis, n=3 and errors bars=standard error of mean (SEM) in **i** and **l**.

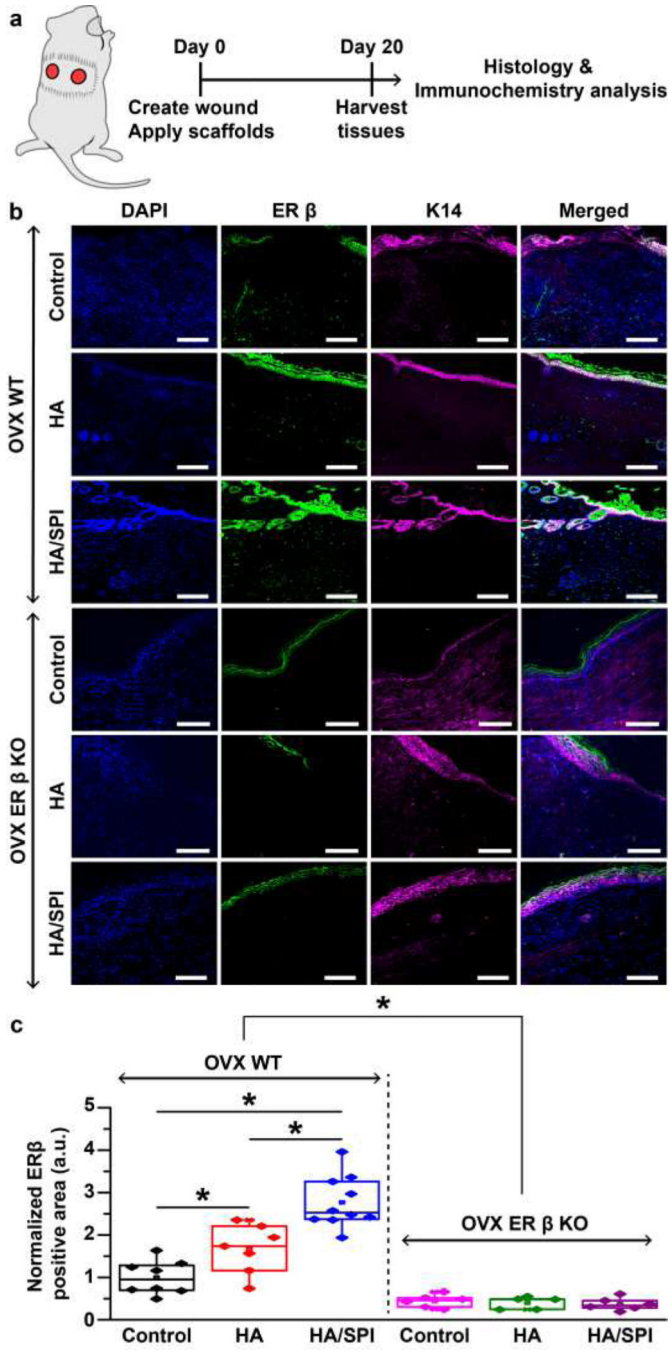

Fig. 2. ER-β expression in mouse skin at day 20 post-injury.

a, Schematic illustration of the experimental timeline. **b**, Immunofluorescence images of day 20 post-injury mouse skin stained with DAPI (for nuclei), anti-ER-β, and anti-K14 (for keratinocytes) antibodies. Scales are 100 μm. **c,** ER-β expression analysis. For statistical analysis, *p<0.05, for OVX WT mice, n=8 for the control group, n=7 for the HA group, n=10 for the HA/SPI group. For OVX ER-β KO mice, n=6 for the control and HA/SPI group, n=5 for the HA group. Box plots with all data points overlapping show data where

edges, middle bars, and whiskers indicated 25^{th} and 75^{th} percentiles, median, 5^{th} and 95^{th} percentiles, respectively.

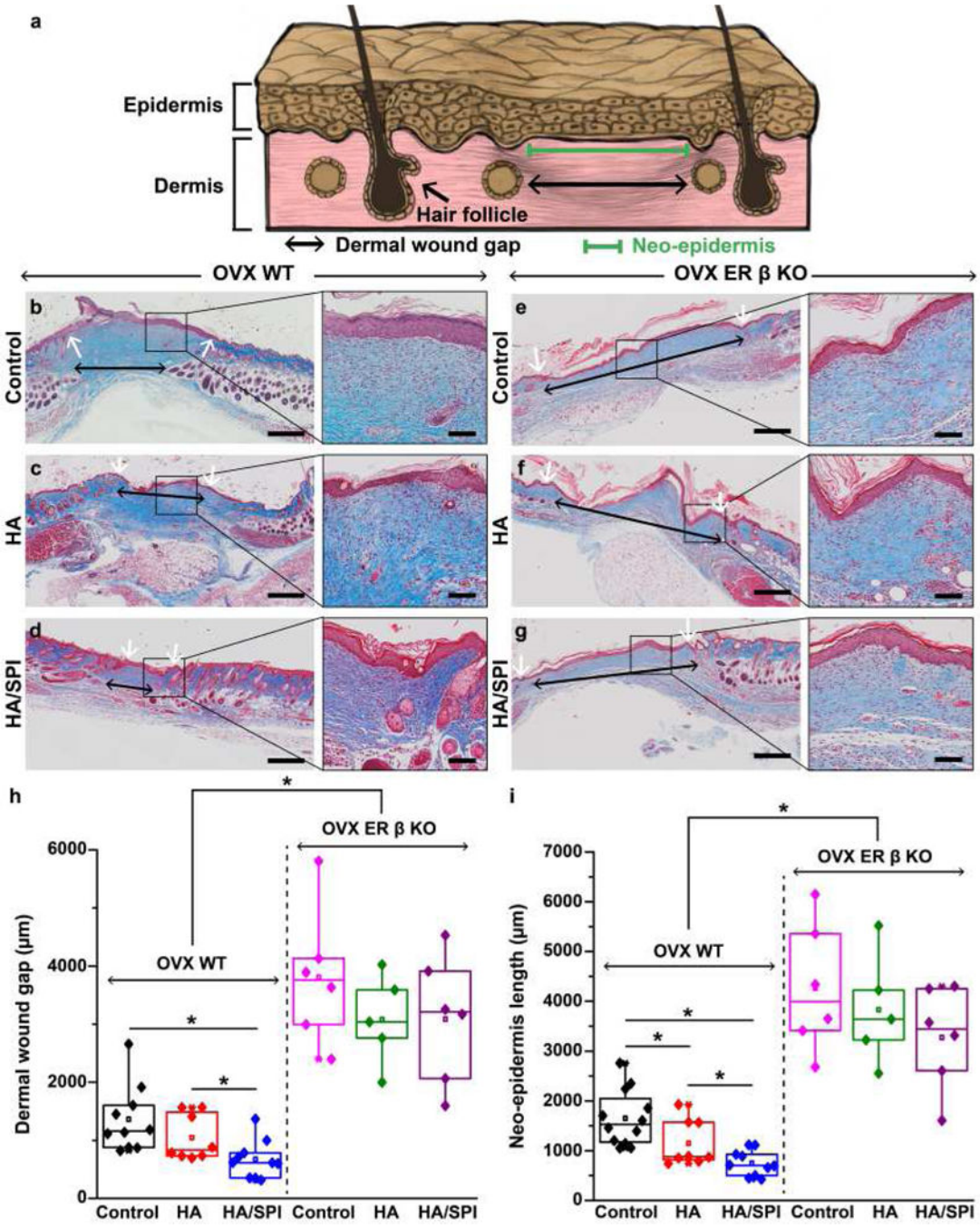

Fig. 3. ***In vivo*** **mouse wound healing and histological studies.**

a, Schematic illustration of the wound healing evaluation parameters. **b–g,** Masson's trichrome images of day 20 post-injury wounds treated with control (no treatment), HA scaffolds, and HA/SPI scaffolds for (**b–d**) OVX WT and (**e–g**) OVX ER-β KO mice with the zoom-in images of healed wounds on the right panels. Black and white arrows indicate dermal wound gaps and the edges of neo-epidermis, respectively. Scales of left and right panels are 500 and 100 μm, respectively. **h–i,** Quantitative analysis of skin tissue repair (**h**, dermal wound gap and **i**, neo-epidermis length) at day 20 post-injury. For statistical analysis,

*p<0.05, For OVX WT mice, n=10 for the control and HA/SPI group, n=8 for the HA group. For OVX ER-β KO mice, n=6 for the control and HA/SPI group, n=5 for the HA group. Box plots with all data points overlapping show data where edges, middle bars, and whiskers indicated 25^{th} and 75^{th} percentiles, median, 5^{th} and 95^{th} percentiles, respectively.

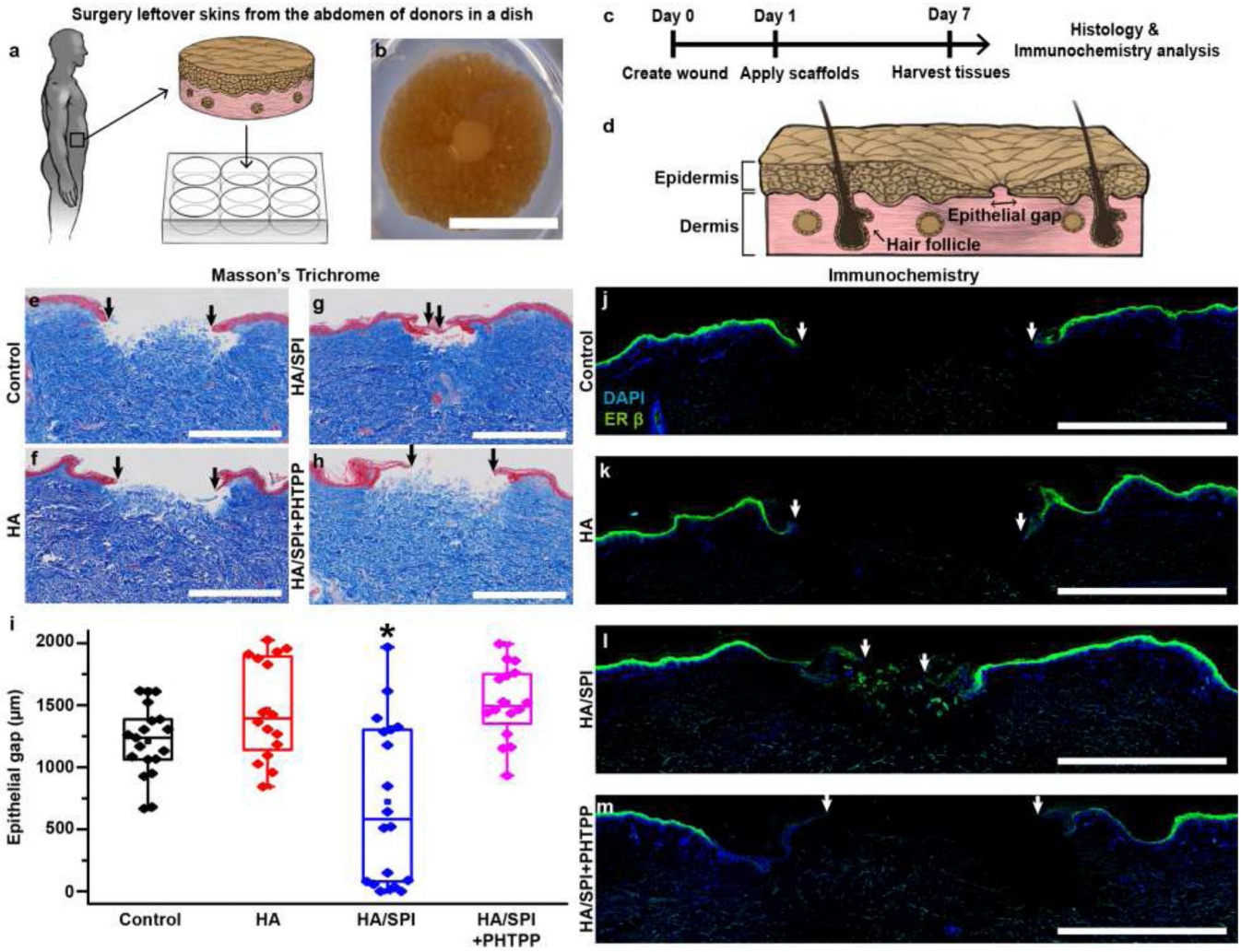

Fig. 4. *Ex vivo* human skin wound healing via ER-β.

a, Schematic illustration of *ex vivo* human skin models. **b–c,** (**b**) Photograph of a wounded human skin biopsy on day 1 prior to scaffold application with (**c**) experimental timeline. **d**, Schematic illustration of the reepithelialization analysis. **e–h,** Masson's trichrome images of day 7 post-injury tissues. The black arrows indicate the edges of the new epithelial tongues. Scales are 1 mm. **i,** Assessment of re-epithelialization analysis at day 7 post-injury. For statistical analysis, *p<0.05, n=9 for the control group, n=8 for the HA group, n=9 for the HA/SPI group, and n=8 for the HA/SPI+PHTPP group, 2 sections per tissue from 2 different patients. Box plots with all data points overlapping show data where edges, middle bars, and whiskers indicated 25th and 75th percentiles, median, 5th and 95th percentiles, respectively. **j–m,** Immunofluorescence images of day 7 post-injury tissues stained with DAPI (for nuclei) and anti-ER-β antibody. The white arrows indicate the edges of the new epithelial tongues. Scales are 1 mm.